Vapor and Pressure Sensors Based on Cellulose Nanofibers and Carbon Nanotubes Aerogel with Thermoelectric Properties

Rajendran Muthuraj, Abhishek Sachan, Mickael Castro*, Jean-François Feller, Bastien Seantier* and Yves Grohens

Dupuy de Lôme Research Institute (IRDL), FRE CNRS 3744, University of Southern Brittany, Rue de Saint Maudé, 56321 Lorient Cedex, France

Received June 20, 2017; Accepted November 14, 2017

ABSTRACT: In this work, thermally insulating and electrically conductive aerogels were prepared from cellulose nanofibers (CNF) and carbon nanotubes (CNTs) by environmentally friendly freeze-drying process. The thermal conductivity of neat CNF aerogel is 24 mW/(m·K) with a density of 0.025 g/cm^3. With the addition of CNTs into CNF aerogel, the electrical conductivity was significantly increased while the thermal conductivity was increased to 38 mW/(m·K). Due to these interesting properties, the Seebeck coefficient and the figure of merit (*ZT*) of the CNF/CNTs aerogels were measured and showed that CNF/CNTs aerogel thermoelectric properties can be improved. The compressibility and electrical resistance of the CNF/CNTs aerogel highlighted its pressure-responsive property. A set of volatile organic compounds (VOCs) were exposed to aerogels to monitor the resistance change. The CNF/CNTs aerogel showed high sensitivity and good response to both nonpolar and polar vapors due to the absorption by both CNF and CNTs networks. The prepared CNF/CNTs aerogel is therefore a good candidate for thermal insulation, thermoelectric material, VOCs sensing, and pressure-sensing applications.

KEYWORDS: CNF/CNTs aerogel, thermal conductivity, pressure sensing, thermoelectric materials, VOCs sensing

1 INTRODUCTION

Aerogels are lightweight and highly porous with a nanometer-scale porosity and with high specific surface area. Therefore, aerogels have drawn increasing attention for use in various fields [1–3], including thermal insulation [4–6], capacitors [7, 8], fire retardant [9], and sensor applications [10–12]. Various inorganic and organic materials have been used to produce aerogels either by freeze-drying or by supercritical drying [13, 14]. Among the organic aerogels, cellulose-based aerogels are attractive materials because of their good mechanical properties, sustainability, and renewability [15]. However, the effective thermal conductivity of cellulose aerogels (0.029–0.030 W/(m·K)) is relatively high. This can be explained by the parallel flux model [16, 17]. In fact, the measured thermal conductivity, called effective thermal conductivity, is the combination of three contributions: the convection in the pores, the conduction through the materials and the radiation of electromagnetic waves through the material. In general, the convection has a negligible effect as the pores are very small [18]. Concerning the conduction, two heat transfers can be observed. On one hand, there is the heat transfer due to the conduction via phonons in the solid phase (later referred to as solid conduction). On the other hand, the heat transfer can be due to the collision between gas molecules (referred to as gas conduction) [19]. Finally, as the material is semi-transparent to electromagentic waves, some heat is transferred via these radiations [16]. It will later be referred to as "radiation" contribution. In the case of aerogels, the pores are quite large. Therefore, the material has a huge effect on gas conduction and radiation. That is the reason why they usually have relatively high effective thermal conductivity. Recently, CO_2 supercritical drying method allowed addressing this drawback. For example, the thermal conductivity of amorphous cellulose aerogels prepared by this method reached lower values than that of air. This is the reason why these materials are called thermal superinsulating material [20]. Lately, Kobayashi *et al*. [5] reported the lowest thermal conductivity for cellulose nanofiber (CNF) aerogels prepared

**Corresponding authors*: bastien.seantier@univ-ubs.fr; mickael.castro@univ-ubs.fr

DOI: 10.7569/JRM.2017.634182

by supercritical drying (0.020 W/(m·K)). CNF aerogels produced by freeze-drying are also promising sustainable materials for thermal insulation because of their low thermal conductivity (0.028 W/(m·K)) [21]. With the aim of reducing aerogel thermal conductivity, it is possible to use thermal opacifiers. These particles are able to absorb photons and to reduce the material radiations contribution of the effective thermal conductivity. Carbonaceous materials have already been deposited on silica aerogels as opacifiers [22]. Therefore, carbon nanotubes (CNTs) addition in CNF aerogel could play a role to decrease the thermal conductivity of resulting aerogels [23]. It can also make the aerogels more electrically conductive and create thermoelectric (TE) materials [24]. Until now, inorganic compounds (e.g., Bi_2Te_3 or bismuth telluride-based alloys) have been used as good TE materials at room temperature. However, their limited availability and complex fabrication process limit their use for industrialization [25, 26]. Organic aerogels with electrically conductive and thermally insulative properties can provide a new route to produce TE materials. Very few researchers have studied aerogel-based material for TE applications. Gordon *et al.* [27] proposed intrinsically electrically conductive poly(3,4-ethylenedioxythiophene):poly(4-styrenesulfonate) (PEDOT:PSS) aerogels as potential TE materials. Graphene and multiwall carbon nanotube-based aerogels have also been studied for such application [28]. These studies concluded that the performance of the resulting aerogels is not suitable for practical TE application.

With unique features such as porous structure, electrical conductivity and high specific surface area, aerogels can be ideal candidates for gas- and pressure-sensing applications [29–31]. Cellulose/CNTs aerogel has been used as volatile organic compound (VOCs) sensors [10]. Noremberg *et al.* [32] recently attempted cellulose/multiwall CNTs-based composite film for gas sensors. However, combining the CNF aerogels with the CNTs is not easy. Therefore, Qi *et al.* [33] dispersed CNTs in cellulose dissolved in aqueous alkaline-urea solution to prepare CNT/cellulose aerogel. The electrical resistance of the CNF/CNTs aerogel was reduced under pressure because of the nanotubes percolation [34]. Moreover, they showed that the electrical conductivity of CNF/CNTs aerogels is increased with increasing CNTs content. The maximum electrical conductivity (2×10^{-3} S/cm) was observed with 25 wt% CNTs [12]. These studies showed the feasibility of developing cellulose aerogel-based sustainable materials for various applications. The present study was aimed at preparing CNF/CNTs aerogel with different CNTs concentrations by environmentally friendly freeze-drying method. The prepared CNF/CNTs aerogels thermal conductivity, electrical conductivity, thermoelectric property, VOCs sensing, and pressure-sensing properties were investigated.

2 MATERIALS AND METHODS

2.1 Materials

A viscous 1 wt% CNF water suspension with 1.3 mmol/g surface charges content was procured from EMPA (Dübendorf, Switzerland). It was prepared via TEMPO-oxidation pretreatment of wood pulp [35]. In order to achieve a required concentration of CNF, osmotic concentration method was used to concentrate the CNF dispersion [36]. The diameter and length of the CNF are 3.85 ± 0.98 nm and 450 nm, respectively [36]. Commercially available aqueous dispersion of unfunctionalized multiwall carbon nanotubes (MWCNTs) were purchased from Nanocyl. The concentration of MWCNT in the aqueous dispersion was 1 mg/100 µl. Hereafter, MWCNTs will be referred to as CNTs.

2.2 Aerogel Preparation

A previous study [36] showed that the aerogel prepared from 2 wt% CNF suspension has better thermal insulation property. Therefore, in this study we have selected 2 wt% CNF suspension to prepare aerogels. Carbon nanotubes (CNTs) were used as thermal opacifier in CNF aerogels. Different concentrations of CNTs related to CNF (1, 5, 10, 15, 20, and 25 wt%) were added in CNF suspension to prepare hydrogels. After incorporation of CNTs into CNF suspension, the mixture was sonicated in a Branson 3510 device (100 W, 40 kHz) for 30 min at 25 °C. The sonicated formulations were poured into an aluminum mold (2 × 2 × 0.39 cm). They have been designed to fit the device used for the thermal conductivity measurement having a volume of 1.578 cm^3. All these samples were frozen at –80 °C for 24 h. Subsequently, a freeze-drying process was performed in a Christ Alpha 1–2 LD Plus freeze dryer at –55 °C with 0.1 mbar pressure. After 48 h, the aerogels are formed. Similary, neat CNTs and neat CNF aerogels were prepared to compare with CNF/CNTs aerogels. At least four samples were prepared for each formulation. The produced monolithic aerogels are represented in Figure 1. They are lightweight (Figure 1a) and mechanically stable (Figure 1b). The morphology will be described more precisely in the coming sections.

2.3 Density and Porosity Measurements

The samples bulk density (ρ_{bulk}) was determined by dividing their weight by their volume. The

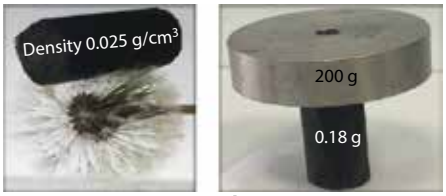

(**a**) (**b**)

Figure 1 Images of monolithic CNF/CNTs aerogels. These aerogels are: (**a**) lighweight, as they do not damage the dandelion and (**b**) mechanically stable, as their shape does not change under a compresive load of 200 g.

measurements were performed with a digital caliper and a Denver Instrument (Model SI-114) balance. The porosity (ε) of the aerogels was calculated by Equation 1, where the relative density is $\rho_{bulk}/\rho_{skeletal}$. The skeletal density ($\rho_{skeletal}$) of the aerogel has been estimated from the proportion of CNF and CNT and their densities. They come from the literature and their values are 1.6 [36] and 2.6 g/cm^3 [37], respectively.

$$\varepsilon(\%) = (1 - (\rho_{bulk}/\rho_{skeletal})) \times 100 = (1 - (\rho_{bulk}/(\%CNF \times \rho_{CNF} + \%CNT \times \rho_{CNT})) \times 100 \quad (1)$$

2.4 Scanning Electron Microscopy

Morphology of the aerogel was observed with a JEOL JSM 6460LV scanning electron microscope (SEM). It was used with an accelerating voltage of 20 kV. The images made are cross sections of the samples. They were obtained after cryo-fracture of the sample in liquid nitrogen. Prior to observing the morphology, the samples were sputtered with a thin gold layer. To get the pore size distribution, SEM images were analyzed with ImageJ version 1.47. At least 100 pores were measured.

2.5 Thermal Conductivity

Thermal conductivity (λ) of the prepared aerogels was measured with the hot strip technique. The conductance (K) of the aerogel is first calculated by the ratio of the dissipated heat through the sample over the temperature difference in both sides of the sample (Equation 2).

$$K = Q/\Delta T = U \times I / (T_2 - T_1) = (U \times V)/(R \times (T_2 - T_1)) \quad (2)$$

More specifically, the cell which contained the material was kept at constant temperature of 19 °C (T1). The other side of the sample had a temperature of T2. T2 was due to a temperature difference coming from the heating of a strip. The dissipated heat is calculated by measuring the Joule effect, i.e., the tension (U, in Volts) times the intensity (V/R, in Amps) passing the strip. U and V are measured with a multimeter, while R is a known resistance equal to 50 Ω. Calibration of the hot strip device is needed to obtain the thermal condcutivity. It was performed using wood, cork, polyurethane foams and polycarbonate samples having thermal conductivity already determined by other techniques. The detailed description of the thermal conductivity equipment setup and calibration is given elsewhere [36, 38].

2.6 Sample Electrical Resistance

In order to measure the electrical properties, a silver lacquer was applied on the opposite side of each sample. The electrical resistance of the material was measured by a Keithley 6517B electrometer at room temperature. The resistance (R_{elec}) was measured three times on each sample and the electrical resistivity (ρ_{elec}) was calculated by Equation 3:

$$\rho_{elec} = R_{elec} \times S/L \quad (3)$$

where S is cross section of the sample (0.789 cm²) and L is length of the sample (2 cm). The electrical resistivity was used to calculate the electrical conductivity of the materials. The electrical conductivity (σ) is equal to the inverse of the electrical resistivity (ρ_{elec}).

2.7 Thermoelectric Measurements

A thermoelectric (TE) material works either with a difference of temperature creating an electrical potential or an electrical potential generating a temperature difference [39]. The TE materials' performance can be measured with the dimensionless figure of merit, ZT, defined by Equation 4:

$$ZT = \sigma \times S^2 \times T/\lambda \quad (4)$$

where σ is the electrical conductivity (S/cm), S is the Seebeck coefficient (μV/K) which is equal to the ratio of ΔV over ΔT, T is the absolute temperature (K), and λ is the thermal conductivity (W/(m·K)) [40]. The Seebeck coefficient was determined via a homemade device. The aerogels' thermoelectric temperature sensing was measured by holding them between two copper bars. Both sides of the samples were heated using two Peltier modules. The temperature difference (ΔT) across the sample was monitored with two thermocouples attached to each side. The voltage (ΔV) generated by temperature difference between the hot and cold side was measured over time. The detailed experimental setup is provided in a previous publication [41].

2.8 Pressure Sensing

Simultaneously measuring the electrical conductivity and compressibility of the aerogels results in

evaluating their pressure-responsive property. A cylindrically shaped aerogel with a diameter of 15 mm and a height of 25 mm was prepared for compression test. The compression tests were performed with an Anton Paar MCR 301 rheometer equipped with parallel plates. The samples were placed between the two circular electrodes and compressed to different strains. Then, the electrical conductivity was measured at each strain.

2.9 Dynamic Vapor Sensing

The CNF/CNTs aerogel was tested for chemoresistive properties using dynamic vapor testing setup. The conducting areogel sensor is developed to work at room temperature. Therefore, the sensor has not been tested at higher temperatures. The aerogel connected with copper wires using silver paint was kept inside a closed rectangular chamber (10 × 10 cm). Aerogel was first exposed to nitrogen bubbling in organic solvents to generate saturated gas for sensing. Then, an alternate cycle of dry nitrogen was carried out for the cleaning of the chamber from solvent vapors. The VOCs selected are common toxic solvent vapors present in the environment. Each cycle was carried out for 5 min at room temperature (20 °C) with relative humidity of 57%.

Sensing device consisted of a mass flow controller, solvent bubbler, programmable electronic valves and Keithley 6517B electrometer connected with LabVIEW software. The change in the resistance of an aerogel was measured by multimeter and data were recorded by software. Flow rate for dry nitrogen was 500 mL/min and 100 mL/min for saturated solvent vapor; both were controlled by mass flow controller. Relative change in aerogel resistance (A_R) was calculated from Equation 5 to compare its response towards different solvent vapors:

$$A_R = (R - R_0) / R_0 \quad (5)$$

where R_0 is initial resistance of sensors in dry nitrogen stream and R is resistance in the presence of solvent vapor.

At saturated conditions, the concentration of VOCs cannot be controlled effectively. Therefore, experiments were carried out using an Owlstone OVG-4 vapor generator and LabVIEW software to test the performance of CNF/CNTs aerogel at low concentration of water vapor and benzene vapor. The flow rate of the vapor was 100 mL/min at 83 °C for both solvents. The concentrations of both solvent vapors were varied from 100 to 17 ppm during the experiment using a spit flow control valve of an OVG-4 oven.

The slope of the curves representing A_R versus the concentration gives the sensitivity of the sensor for VOCs. The sensitivity of sensors is defined as the increase in sensors amplitude when a unit change is applied in analyte concentration [42].

In order to assess the efficiency of the sensors with low concentration of vapor molecules, the signal-to-noise ratio (SNR) of the sensors was calculated during sensing of VOCs [43]. The SNR of sensors is calculated by using Equation 6:

$$SNR = A_R / \sigma_{baseline} \quad (6)$$

where A_R is response of aerogel obtained after exposure to solvent and $\sigma_{baseline}$ represents the standard deviation in baseline resistance of sensor before the analyte delivery. The concentration of the solvents can be detectable by the sensors if its SNR value is higher than 3 (SNR > 3).

3 RESULTS AND DISCUSSIONS

3.1 Aerogel Structure and Morphology

The cross-sectional morphology images of the prepared aerogels is shown in Figure 2. It can be observed that the CNF aerogel morphology was slightly affected after incorporation of different concentrations of CNTs. CNF aerogel (Figure 2a) showed a filmlike structure which is commonly observed for CNF aerogels prepared with more than 0.5 wt% concentration [36]. The CNF aerogels with carbon nanotubes (Figure 2b and 2c) showed similar sheetlike structures compared to neat CNF aerogel. The insert in Figure 2b shows that some CNTs are absorbed at the surface of CNF filmlike structure. The SEM image analysis revealed that the neat CNF aerogels have an average pore size of 26 ± 11 μm. Concerning the CNF/CNTs aerogels, the pore size is 23 ± 11 μm. This slight decrease in the pore size could be due to the aggregation of carbon nanotubes on the CNF films (see insert in Figure 2b). The preparation of CNT aerogels highlights another possibility. Figure 2d represents the SEM images of the cross section of CNT aerogels. They showed that CNTs are also able to form film via freeze-drying. Therefore, the reduction of the pore size can also be due to the formation of new pore walls with CNTs.

The density of the aerogels versus the CNT concentration is presented in Figure 3. The density of the CNF aerogel is 0.025 g/cm^3 while the density of CNTs aerogel is 0.035 g/cm^3. Due to the higher density of CNTs, the density of CNF/CNTs aerogel increased with increasing CNTs content. The porosity of the neat CNF aerogel and CNTs aerogel, calculated from Equation 1, is 98.43 and 98.65%, respectively. This high porosity is in complete agreement with the large pore sizes measured on SEM images. When different concentrations

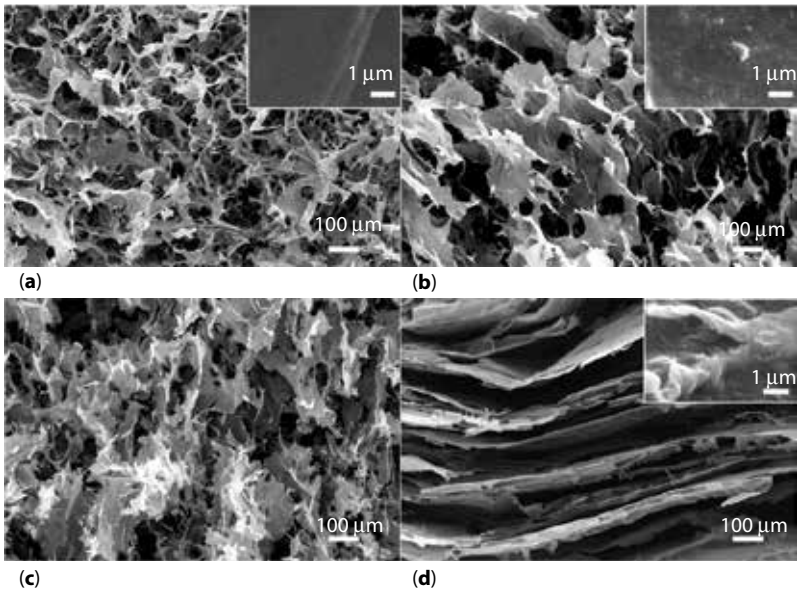

Figure 2 SEM images of the aerogel cross section: (**a**) neat CNF, (**b**) CNF/CNTs (95/5 wt%), (**c**) CNF/CNTs (75/25 wt%), and (**d**) neat CNTs. The inserts are 100 times magnification of the pore wall. They reveal the fine interaction between CNF and CNTs. In Figure 2a, smooth pore walls are observed. In Figure 2b, CNTs are present at the surface of CNF pore walls. In Figure 2d, the pore walls are formed by CNT entanglement.

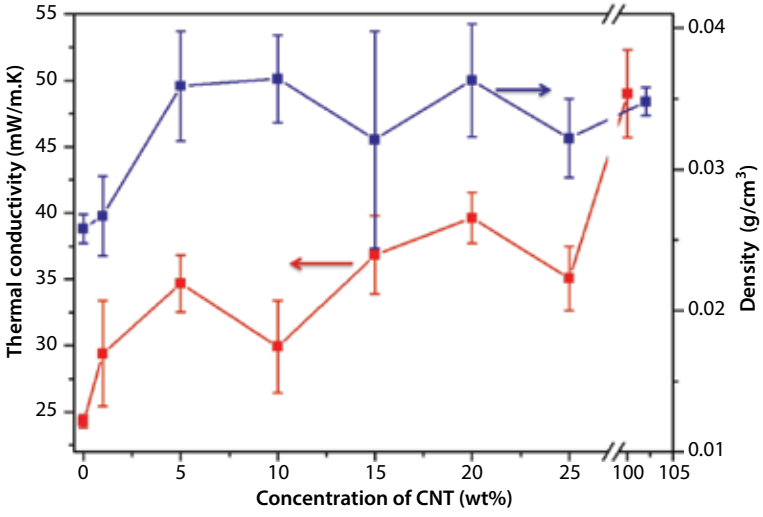

Figure 3 Thermal conductivity and density of CNF/CNTs aerogels versus the CNT content.

of CNTs were incorporated into CNF aerogel, the porosity of the resulting aerogel was not affected significantly. The crosslinked polysaccharide-based aerogels have lower porosities (85–41%) and higher densities (0.25–0.85 g/cm^3) because, when crosslinking, such a network can undergo a large shrinkage, i.e., 20–60% [15, 36]. The absence of crosslinking in our system can explain why it has higher porosity and lower density compared to crosslinked polysaccharide aerogels.

3.2 Thermal Conductivity

The thermal conductivity of the aerogels is represented in Figure 3. For neat CNF aerogel, the value is around 24 mW/(m·K), which is slightly lower than the thermal conductivity of air [27]. The observed CNF thermal conductivity is similar to pectin aerogels while superior to some other polysaccharide aerogels [44–46]. It was expected that the CNTs could act as thermal opacifier in CNF aerogels. CNTs were

used to reduce the radiation contribution of the thermal conductivity in CNF/CNTs aerogels. However, the thermal conductivity of the CNF/CNTs aerogel was slightly increased from 2 to 25 wt% CNTs incorporation (Figure 3). Indeed, it has been commonly observed that a higher density for aerogels induces higher solid conduction. Thus, the thermal conductivity of the resulting aerogel increases [47]. The maximum thermal conductivity (38 mW/(m·K)) was observed with 20 wt% CNTs incorporation. This observed deviation in the thermal conductivity of the CNF/CNTs aerogel could be due to the reasons previously discussed in the SEM image analysis. On one hand, the formation of CNT pore walls may cause increased solid conduction. On the other hand, the aggregation of the CNT on CNF pore walls can induce higher solid conduction because of the intrinsic CNT thermal conduction (Figure 2). Moreover, the first quick increase to 5 wt% of CNT followed by a slight increase of the thermal conductivity may be attributed to the percolation thresholds of the CNT in the resulting aerogels (Figure 2). From the thermal conductivity result, it can be concluded that in order to achieve CNF/CNTs aerogels with a low thermal conductivity, a low concentration of CNT should be incorporated into the CNF aerogels.

3.3 Electrical Resistance and Electrical Conductivity

The resistance and the electrical conductivity of the aerogels as a function of the CNTs content are given in Figure 4. The CNF/CNTs aerogel with 1 wt% CNTs showed electrically insulating behavior with a high resistance value. When 5 wt% CNTs was incorporated into CNF aerogel, there was a significant improvement in electrical conductivity of the resulting aerogel. The increased electrical conductivity of CNF/CNTs aerogels is attributed to the charge carriers injected by CNTs. It was observed that the CNF/CNTs aerogel with 25 wt% CNTs had maximum electrical conductivity (0.029 S/cm). But it is still lower than the neat CNTs aerogel electrical conductivity (0.045 S/cm). The observed electrical conductivity of CNF/CNTs aerogel is much higher than the literature cellulose-functionalized CNTs composite aerogels [12, 34] as well as intrinsically conductive PEDOT:PSS/acid treated carbon nanotube aerogels [48]. This could be due to the better dispersion of CNTs in the CNF matrix.

3.4 Thermoelectric Properties

Because of previous results, we thought it would be interesting to examine the Seebeck coefficient of these aerogels to evaluate their potential as TE material. Due to their p-type characteristic, all the aerogels showed positive Seebeck coefficient values. The Seebeck coefficient value of neat CNTs aerogel was around 11 μV/K. There was no significant difference in CNF/CNTs aerogel Seebeck coefficient when increasing the CNTs content. The maximum Seebeck coefficient (15 μV/K) value was observed for CNF/CNTs aerogel with 25 wt% CNTs at room temperature. This Seebeck coefficient is comparable to intrinsically conductive PEDOT:PSS aerogels [27] while being lower than the n-type polyacetylenes/polyanilines value [25]. Using the observed Seebeck coefficient values, ZT was evaluated. Its value was slightly increased with increasing CNTs content up to 25 wt%. Yet, the value of the ZT was quite low. The maximum ZT value (0.0547×10^{-8})

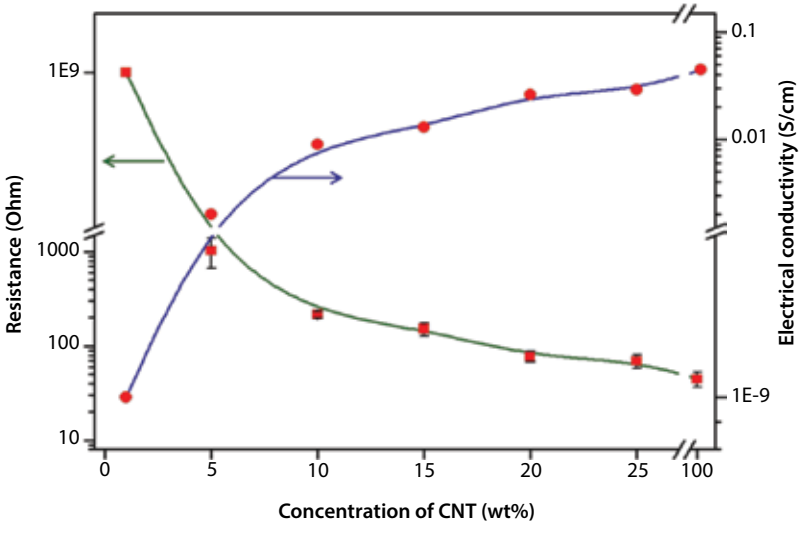

Figure 4 Resistance and electrical conductivity of CNF/CNTs aerogels versus the CNT content.

was observed for CNF/25 wt% CNTs aerogel while it was 0.0343×10^{-8} for neat CNTs aerogel.

3.5 Vapor Sensing

Though the TE performances were not good enough for applications, the developed aerogels exhibit a certain electrical conductivity. Therefore, CNF/CNTs areogels have been tested for vapor-sensing properties. Chemoresistive response of CNF/CNTs aerogel is presented in Figure 5b for 10 different VOCs, including water. Average maximum responses for 4 cycles are shown in Figure 5a. Aerogel exhibited a maximum response for water and chloroform. The maximum response was observed towards chloroform. The second highest response was found once exposed to water. In order to better understand these results, we hypothesized possible VOC sensing mechanisms for CNF/CNTs sensor, which is schematically represented in Figure 6 [49]. One possibility is the swelling of the CNF structure (big plain circle in Figure 6). It induces the disconnection of the

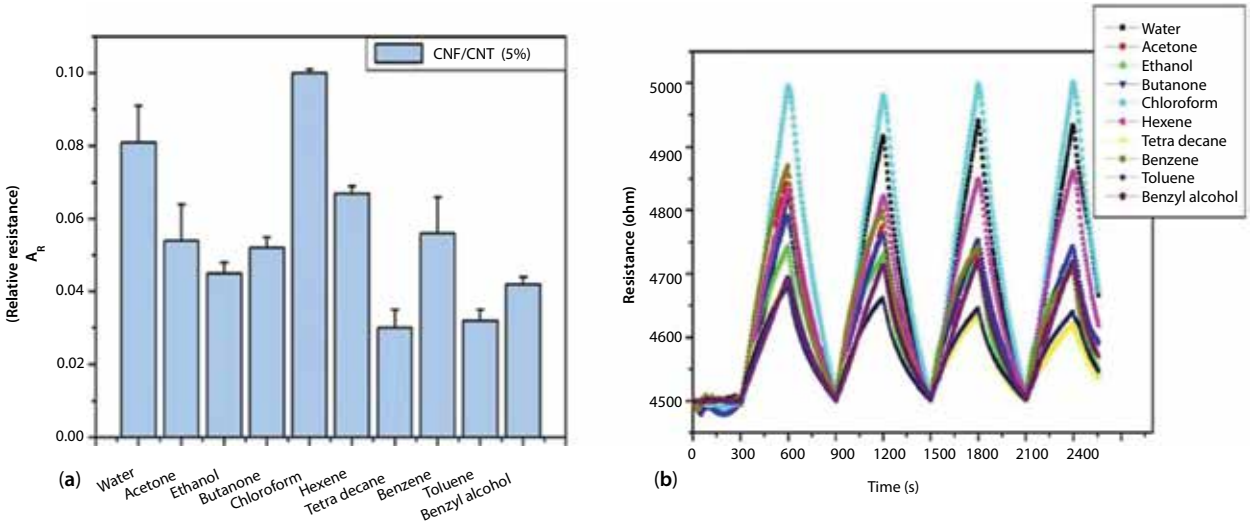

Figure 5 VOCs sensing response of the CNF/CNTs (5%) aerogel: (**a**) representation of the mean relative resistance of the sensor over the 4 cycles represented in Figure 5b. Error bars are the standard deviation. (**b**) Row data of the sensor resistance for 10 VOCs over the 4-cycle experiment.

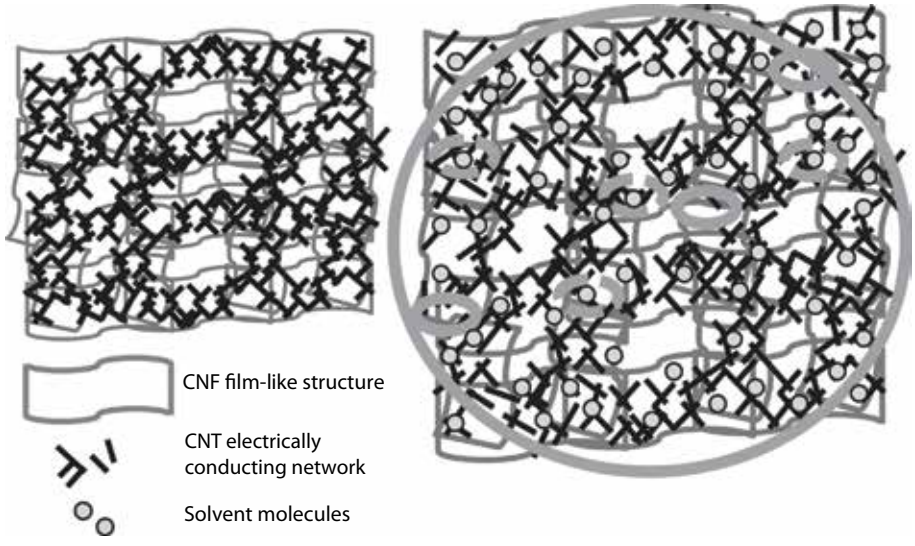

Figure 6 Mechanism of CNF/CNTs aerogel vapor sensing in the presence of solvent vapors. If the solvent has preferential interactions with CNFs, then the structure may swell (big plain circle) and induce the disconnection of the CNTs (small plain circles). If the solvent interacts more with CNTs, it may disrupt the CNT/CNT connections (dashed circles). In both case, it induces a decrease of the electrical conduction.

CNTs (small plain circles in Figure 6) and an increase of the electrical resistivity of the aerogel. Another possibility is the disturbance of CNT/CNT connection because of the presence of solvent molecules (dashed circles in Figure 6). With these hypotheses, we speculate the following to explain our results. On one hand, for chloroform, the maximum response is due to its high concentration present at room temperature. The chloroform is known to have good swelling effects on polymers. Thus, chloroform absorption at CNF surface increased the resistance of conducting network very rapidly, as shown in Figure 5b [50–52]. On the other hand, the hydrophilic nature of CNF leads to the absorption of water molecules at conducting junctions of CNTs [53]. The CNF film swelling and the disconnection of CNTs due to the presence of water molecules induces a decrease of the electrical conduction. For other nonpolar VOCs, responses are lower because of their lower interaction with cellulosic fibers and/or CNTs.

To study the sensitivity of the sensor, the response of one non-interacting (benzene) and one interacting (water) solvent was carried out at 4 different concentrations (at 100, 50, 25 and 17 ppm). The raw signals are presented in Figure 7b and 7c for benzene and water respectively. For benzene, fewer variations were observed in the response when concentration was varied compared to water. To evaluate the difference in behavior between both solvents, A_R is plotted with respect to concentrations (Figure 7a). It can be seen that the sensitivity of CNF/CNT aerogel was 1.642 × 10^{-5} ppm^{-1} and 8.443 × 10^{-5} ppm^{-1} for benzene and water, respectively. Some studies have already shown that sensors may have enhanced response when solvent vapors are mixed with a large amount of water vapors [54]. However, due to the high affinity of CNF

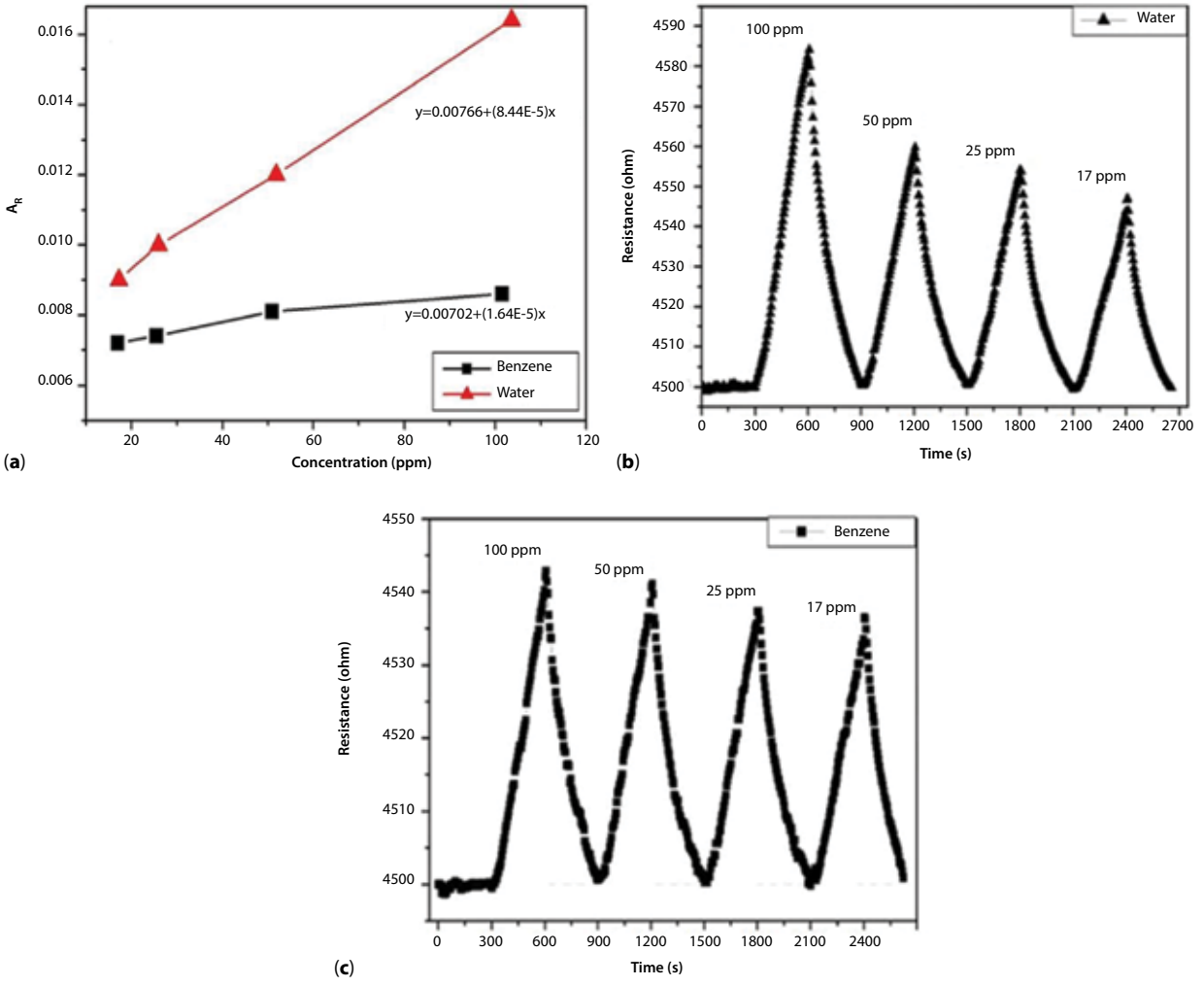

Figure 7 (**a**) Sensitivity curve of aerogel at various concentrations (100 to 17 ppm) of water and benzene. It corresponds to the evolution of the relative resistance of the sensor versus the concentration of the solvent vapors. (**b, c**) The raw resistance of the sensor versus time for benzene and water, respectively, at various concentrations (100 to 17 ppm).

towards water, a large amount of water can disturb the conducting network of CNTs in CNF/CNTs aerogel. Therefore, the sensing response of the CNF/CNTs aerogels with high humidity was not performed in this study. Though not very selective for any specific solvent vapors, CNF/CNTs sensor can detect a wide range of VOCs present as pollutants in the environment. Besides thermoelectric properties, the CNF/CNTs sensor can be used to monitor VOC content in closed environments such as inside buildings, offices and homes.

Finally, the efficiency of the sensor was evaluated. SNR values were 4.6 and 5.7 for water and benzene, respectively. It illustrates the ability of CNF/CNTs aerogels to correctly sense down to the concentration of 15 ppm for both solvents. However, it was difficult to sense VOCs below 15 ppm with this aerogel. Yet, this benzene detection limit (15 ppm) is much lower than that of the human nose (60 ppm) in air [55]. The stability of signals was also calculated from the standard deviation of the baseline. The $\sigma_{baseline}$ was around 0.002, which is very small as compared to the signals. The maximum deviation was less than 10% of its average signal value. Thus, the signals generated by CNF/CNTs areogel were quite stable at room temperature.

3.6 Pressure Sensing

Pressure-responsive properties of the aerogel were obtained from their combined compressible properties and electrical resistance measurement. The relative electrical resistance, compressive stress, and compressive strain of the CNF/CNTs (95/5 wt%) aerogel are shown in Figure 8. Ordinarily, electrical conductivity increases when the contact between the electrically conductive particles increases. As expected, the relative electrical resistance of the CNF/CNTs aerogel

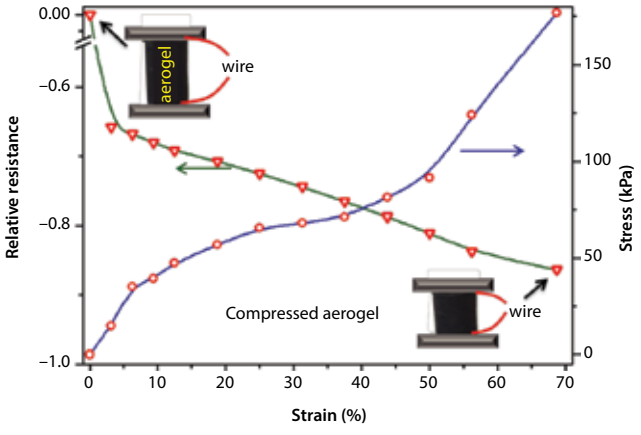

Figure 8 Relative resitance and stress of CNF/CNTs (95/5 wt%) aerogels with respect to strain.

gradually decreased with increasing compressive strain and stress. This behavior is attributed to an increasing number of contacts in the continuous conductive CNTs network. The lowest relative electrical resistance was observed when the strain and stress reached 70% and ~177 kPa, respectively. This observation was in good agreement with aerographite relative electrical resistance change with respect to compressive strain [56]. Zhou *et al.* [57] also observed such a behavior in CNF/polypyrrole/silver nanoparticles aerogels with increasing compressive strain up to 90%. Therefore, this kind of electrically conductive aerogels under compressive strain could be used for pressure-sensing material applications.

4 CONCLUSIONS

In conclusion, an efficient, low-cost, and environmentally friendly process was used to produce CNF/CNTs aerogels. The thermal conductivity, themoelectrical property, electrical conductivity, chemical vapor-sensing, and pressure-sensing properties were investigated. With the addition of CNTs into CNF aerogel, the thermal conductivity and density of the resulting aerogels were slightly increased as compared to neat CNF aerogel. At the same time, electrically conductive aerogels were obtained. Therefore, the CNF/CNTs aerogels were tested for TE properties. The Seebeck and ZT values appeared too low for the real application requirements. Therefore, these values should be effectively modified by increasing electrical conductivity and reducing the thermal conductivity of CNF/CNTs aerogels. Yet, the CNF/CNTs aerogels showed relative electrical resistance change towards chemical vapors because of their porous structure, which can efficiently and directly interact with vapors. The electrical conductivity of the aerogel was increased under compressive stress because of the formation of continuous CNT networks. Finally, all these results illustrate a facile and intriguing preparation strategy for aerogels for multifunctional material applications. The prepared CNF/CNTs aerogel could be used as a platform to develop a new class of TE material by incorporating intrinsically conductive polymers and/or by using a reductive treatment.

REFERENCES

1. K.S. Mikkonen, K. Parikka, A. Ghafar, and M. Tenkanen, Prospects of polysaccharide aerogels as modern advanced food materials. *Trends Food Sci. Technol.* **34**(2), 124–136 (2013).
2. H. Maleki, L. Durães, C.A. García-González, P. del Gaudio, A. Portugal, and M. Mahmoudi, Synthesis and

biomedical applications of aerogels: Possibilities and challenges. *Adv. Colloid Interface Sci.* **236**, 1–27 (2016).
3. A. Demilecamps, C. Beauger, C. Hildenbrand, A. Rigacci, and T. Budtova, Cellulose–silica aerogels. *Carbohydr. Polym.* **122**, 293–300 (2015).
4. S. Takeshita and S. Yoda, Chitosan aerogels: Transparent, flexible thermal insulators. *Chem. Mater.* **27**(22), 7569–7572 (2015).
5. Y. Kobayashi, T. Saito, and A. Isogai, Aerogels with 3D ordered nanofiber skeletons of liquid-crystalline nanocellulose derivatives as tough and transparent insulators. *Angew. Chem. Int. Ed.* **53**(39), 10394–10397 (2014).
6. C. Rudaz, R. Courson, L. Bonnet, S. Calas-Etienne, H. Sallée, and T. Budtova, Aeropectin: Fully biomass-based mechanically strong and thermal superinsulating aerogel. *Biomacromolecules* **15**(6), 2188–2195 (2014).
7. G. Zu, J. Shen, L. Zou, F. Wang, X. Wang, Y. Zhang, and X. Yao, Nanocellulose-derived highly porous carbon aerogels for supercapacitors. *Carbon* **99**, 203–211 (2016).
8. J. Tian, D. Peng, X. Wu, W. Li, H. Deng, and S. Liu, Electrodeposition of Ag nanoparticles on conductive polyaniline/cellulose aerogels with increased synergistic effect for energy storage. *Carbohydr. Polym.* **156**, 19–25 (2017).
9. B. Wicklein, A. Kocjan, G. Salazar-Alvarez, F. Carosio, G. Camino, M. Antonietti, and L. Bergström, Thermally insulating and fire-retardant lightweight anisotropic foams based on nanocellulose and graphene oxide. *Nat. Nano.* **10**(3), 277–283 (2015).
10. H. Qi, J. Liu, J. Pionteck, P. Pötschke, and E. Mäder, Carbon nanotube–cellulose composite aerogels for vapour sensing. *Sens. Actuators B Chem.* **213**, 20–26 (2015).
11. J. Zou, J. Liu, A.S. Karakoti, A. Kumar, D. Joung, Q. Li, S.I. Khondaker, S. Seal, and L. Zhai, Ultralight multiwalled carbon nanotube aerogel. *ACS Nano* **4**(12), 7293–7302, (2010).
12. M. Wang, I.V. Anoshkin, A.G. Nasibulin, R.H. Ras, J. Laine, E.I. Kauppinen, and O. Ikkala, Electrical behaviour of native cellulose nanofibril/carbon nanotube hybrid aerogels under cyclic compression. *RSC Adv.* **6**(92), 89051–89056 (2016).
13. H. Maleki, Recent advances in aerogels for environmental remediation applications: A review. *Chem. Eng. J.* **300**, 98–118 (2016).
14. S. Nardecchia, D. Carriazo, M.L. Ferrer, M.C. Gutierrez, and F. del Monte, Three dimensional macroporous architectures and aerogels built of carbon nanotubes and/or graphene: Synthesis and applications. *Chem. Soc. Rev.* **42**(2), 794–830 (2013).
15. F. Fischer, A. Rigacci, R. Pirard, S. Berthon-Fabry, and P. Achard, Cellulose-based aerogels. *Polymer* **47**(22), 7636–7645 (2006).
16. H.-P. Ebert, Thermal properties of aerogels, in *Aerogels Handbook*, pp. 537–564, Springer, New York (2011).
17. J. Fricke, Aerogels—A fascinating class of high-performance porous solids, in *Aerogels*, pp. 2–19, Springer, Berlin, Heidelberg (1986).
18. M. Venkataraman, R. Mishra, T.M. Kotresh, J. Militky, and H. Jamshaid, Aerogels for thermal insulation in high-performance textiles. *Text. Prog.* **48**(2), 55–118 (2016).
19. J. Fricke and A. Emmerling, Aerogels—Preparation, properties, applications. *Struct. Bond.* **77**, 37–87 (1992).
20. F. Ayadi, B. Martín-García, M. Colombo, A. Polovitsyn, A. Scarpellini, L. Ceseracciu, I. Moreels, and A. Athanassiou, Mechanically flexible and optically transparent three-dimensional nanofibrous amorphous aerocellulose. *Carbohydr. Polym.* **149**, 217–223 (2016).
21. D. Bendahou, A. Bendahou, B. Seantier, Y. Grohens, amd H. Kaddami, Nano-fibrillated cellulose-zeolites based new hybrid composites aerogels with super thermal insulating properties. *Ind. Crops Prod.* **65**, 374–382 (2015).
22. D. Lee, P.C. Stevens, S.Q. Zeng, and A.J. Hunt, Thermal characterization of carbon-opacified silica aerogels. *J. Non-Cryst. Solids* **186**, 285–290 (1995).
23. H. Yu, D. Liu, Y. Duan, and Z. Yang, Applicability of the effective medium theory for optimizing thermal radiative properties of systems containing wavelength-sized particles. *Int. J. Heat Mass Transf.* **87**, 303–311 (2015).
24. M.A. Kamarudin, S.R. Sahamir, R.S. Datta, B.D. Long, M.F. Mohd Sabri, and S. Mohd Said, A review on the fabrication of polymer-based thermoelectric materials and fabrication methods. *Sci. World J.* DOI: 10.1155/2013/713640 (2013).
25. B. Russ, A. Glaudell, J.J. Urban, M.L. Chabinyc, and R.A. Segalman, Organic thermoelectric materials for energy harvesting and temperature control. *Nat. Rev. Mater.* **1**, 16050 (2016).
26. N. Massonnet, A. Carella, O. Jaudouin, P. Rannou, G. Laval, C. Celle, and J.-P. Simonato, Improvement of the Seebeck coefficient of PEDOT:PSS by chemical reduction combined with a novel method for its transfer using free-standing thin films. *J. Mater. Chem. C* **2**(7), 1278283 (2014).
27. M.P. Gordon, E.W. Zaia, P. Zhou, B. Russ, N.E. Coates, A. Sahu, and J.J. Urban, Soft PEDOT:PSS aerogel architectures for thermoelectric applications. *J. Appl. Polym. Sci.* **134**(3), 44070 (2017).
28. L. Zhao, X. Sun, Z. Lei, J. Zhao, J. Wu, Q. Li, and A. Zhang, Thermoelectric behavior of aerogels based on graphene and multi-walled carbon nanotube nanocomposites. *Compos. Part B Eng.* **83**, 317–322 (2015).
29. M. Knite, V. Teteris, A. Kiploka, and J. Kaupuzs, Polyisoprene-carbon black nanocomposites as tensile strain and pressure sensor materials. *Sens. Actuators Phys.* **110**(1), 142–149 (2004).
30. M. Knite, K. Ozols, G. Sakale, and V. Teteris, Polyisoprene and high structure carbon nanoparticle composite for sensing organic solvent vapours. *Sens. Actuators B Chem.* **126**(1), 209–213 (2007).
31. K.M. Tripathi, T. Kim, D. Losic, and T.T. Tung, Recent advances in engineered graphene and composites for detection of volatile organic compounds (VOCs) and non-invasive diseases diagnosis. *Carbon* **110**, 97–129 (2016).
32. B.S. Noremberg, R.M. Silva, O.G. Paniz, J.H. Alano, M.R.F. Gonçalves, S.I. Wolke, J. Labidi, A. Valentini, and N.L. V Carreño, From banana stem to conductive paper: A capacitive electrode and gas sensor. *Sens. Actuators B Chem.* **240**, 459–467 (2017).

33. H. Qi, E. Mader, and J. Liu, Electrically conductive aerogels composed of cellulose and carbon nanotubes. *J. Mater. Chem. A* **1**(34), 9714–9720 (2013).
34. M. Wang, I. V Anoshkin, A.G. Nasibulin, J.T. Korhonen, J. Seitsonen, J. Pere, E.I. Kauppinen, R.H.A. Ras, and O. Ikkala, Modifying native nanocellulose aerogels with carbon nanotubes for mechanoresponsive conductivity and pressure sensing, *Adv. Mater.* **25**(17), 2428–2432 (2013).
35. T. Saito, Y. Nishiyama, J.-L. Putaux, M. Vignon, and A. Isogai, homogeneous suspensions of individualized microfibrils from TEMPO-catalyzed oxidation of native cellulose. *Biomacromolecules* **7**(6), 1687–1691 (2006).
36. C. Jiménez-Saelices, B. Seantier, B. Cathala, and Y. Grohens, Spray freeze-dried nanofibrillated cellulose aerogels with thermal superinsulating properties. *Carbohydr. Polym.* **157**, 105–113 (2017).
37. M.F.L. De Volder, S.H. Tawfick, R.H. Baughman, and A.J. Hart, Carbon nanotubes: Present and future commercial applications. *Science* **339**(6119), 535–539 (2013).
38. B. Seantier, D. Bendahou, A. Bendahou, Y. Grohens, and H. Kaddami, Multi-scale cellulose based new bio-aerogel composites with thermal super-insulating and tunable mechanical properties. *Carbohydr. Polym.* **138**, 335–348 (2016).
39. D.D.L. Chung, Composites get smart. *Mater. Today* **5**(1), 30–35 (2002).
40. A. Dey, O.P. Bajpai, A.K. Sikder, S. Chattopadhyay, and M.A. Shafeeuulla Khan, Recent advances in CNT/graphene based thermoelectric polymer nanocomposite: A proficient move towards waste energy harvesting. *Renew. Sustain. Energy Rev.* **53**, 653–671 (2016).
41. T.T. Tung, C. Pham-Huu, I. Janowska, T. Kim, M. Castro, and J.-F. Feller, Hybrid films of graphene and carbon nanotubes for high performance chemical and temperature sensing applications. *Small* **11**(28), 3485–3493 (2015).
42. J. Li, Y. Lu, Q. Ye, M. Cinke, J. Han, and M. Meyyappan, Carbon nanotube sensors for gas and organic vapor detection. *Nano Lett.* **3**(7), 929–933 (2003).
43. S. Nag, L. Duarte, E. Bertrand, V. Celton, M. Castro, V. Choudhary, P. Guegan, and J.F. Feller, Ultrasensitive QRS made by supramolecular assembly of functionalized cyclodextrins and graphene for the detection of lung cancer VOC biomarkers. *J. Mater. Chem. B* **2**(38), 6571–6579 (2014).
44. G. Tkalec, Z. Knez, and Z. Novak, Formation of polysaccharide aerogels in ethanol. *RSC Adv.* **5**(94), 77362–77371 (2015).
45. G. Tkalec, R. Kranvogl, A.P. Uzunalić, Ž. Knez, and Z. Novak, Optimisation of critical parameters during alginate aerogels' production. *J. Non-Cryst. Solids* **443**,112–117 (2016).
46. T.O.J. Blomfeldt, F. Nilsson, T. Holgate, J. Xu, E. Johansson, and M.S. Hedenqvist, Thermal conductivity and combustion properties of wheat gluten foams. *ACS Appl. Mater. Interfaces* **4**(3), 1629–1635 (2012).
47. O.A. Madyan, M. Fan, L. Feo, and D. Hui, Physical properties of clay aerogel composites: An overview. *Compos. Part B Eng.* **102**, 29–37 (2016).
48. X. Zhang, J. Liu, B. Xu, Y. Su, and Y. Luo, Ultralight conducting polymer/carbon nanotube composite aerogels. *Carbon* **49**(6), 1884–1893 (2011).
49. J.F. Feller, N. Gatt, B. Kumar, and M. Castro, Selectivity of chemoresistive sensors made of chemically functionalized carbon nanotube random networks for volatile organic compounds (VOC). *ChemoSensors* **2**, 26–40 (2014).
50. B. Kumar, M. Castro, and J.F. Feller, Tailoring the chemoresistive response of self-assembled polysaccharide-CNT sensors by chain conformation at tunnel junctions. *Carbon* **50**(10), 3627–3634 (2012).
51. B. Kumar, M. Castro, and J.F. Feller, Controlled conductive junction gap for chitosan–carbon nanotube quantum resistive vapour sensors. *J. Mater. Chem.* **22**(21), 10656–10664 (2012).
52. B. Kumar, J.F. Feller, M. Castro, and J. Lu, Conductive bio-polymer nano-composites (CPC): Chitosan-carbon nanotube transducers assembled via spray layer-by-layer for volatile organic compound sensing. *Talanta* **81**(3), 908–915 (2010).
53. B. Kumar, M. Castro, and J.F. Feller, Controlled conductive junction gap for chitosan-carbon nanotube quantum resistive vapour sensors. *J. Mater. Chem.* **22**(21), 10656–10664 (2012).
54. S. Nag, A. Sachan, M. Castro, V. Choudhary, and J.F. Feller, Spray layer-by-layer assembly of POSS functionalized CNT quantum chemo-resistive sensors with tuneable selectivity and ppm resolution to VOC biomarkers. *Sens. Actuators B Chem.* **222**, 362–373 (2016).
55. *Http://desnhgovorganizationcommissionerpipfactsheetsard-documentsard-Ehp-3pdf*. (2017).
56. S. Garlof, M. Mecklenburg, D. Smazna, Y.K. Mishra, R. Adelung, K. Schulte, and B. Fiedler, 3D carbon networks and their polymer composites: Fabrication and electromechanical investigations of neat aerographite and aerographite-based PNCs under compressive load. *Carbon* **111**, 103–112 (2017).
57. S. Zhou, M. Wang, X. Chen, and F. Xu, Facile template synthesis of microfibrillated cellulose/polypyrrole/silver nanoparticles hybrid aerogels with electrical conductive and pressure responsive properties. *ACS Sustain. Chem. Eng.* **3**(12), 3346–3354 (2015).

